AMERICAN SOCIETY FOR MICROBIOLOGY | Molecular and Cellular Biology®

RESEARCH ARTICLE

# Proteomics Screen Identifies Class I Rab11 Family Interacting Proteins as Key Regulators of Cytokinesis

**Carl Laflamme,[a]* Jacob A. Galan,[a]* Khaled Ben El Kadhi,[a] Antoine Méant,[a] Carlos Zeledon,[a] Sébastien Carréno,[a,b] Philippe P. Roux,[a,b] Gregory Emery[a,b]**

Institute for Research in Immunology and Cancer (IRIC), Université de Montréal, Montréal, Québec, Canada[a]; Department of Pathology and Cell Biology, Faculty of Medicine, Université de Montréal, Montréal, Québec, Canada[b]

**ABSTRACT** The 14-3-3 protein family orchestrates a complex network of molecular interactions that regulates various biological processes. Owing to their role in regulating the cell cycle and protein trafficking, 14-3-3 proteins are prevalent in human diseases such as cancer, diabetes, and neurodegeneration. 14-3-3 proteins are expressed in all eukaryotic cells, suggesting that they mediate their biological functions through evolutionarily conserved protein interactions. To identify these core 14-3-3 client proteins, we used an affinity-based proteomics approach to characterize and compare the human and *Drosophila* 14-3-3 interactomes. Using this approach, we identified a group of Rab11 effector proteins, termed class I Rab11 family interacting proteins (Rab11-FIPs), or Rip11 in *Drosophila*. We found that 14-3-3 binds to Rip11 in a phospho-dependent manner to ensure its proper subcellular distribution during cell division. Our results indicate that Rip11 plays an essential role in the regulation of cytokinesis and that this function requires its association with 14-3-3 but not with Rab11. Together, our results suggest an evolutionarily conserved role for 14-3-3 in controlling Rip11-dependent protein transport during cytokinesis.

**KEYWORDS** 14-3-3, cell division, cytokinesis, proteomics, vesicular trafficking

The evolutionarily conserved 14-3-3 family of pSer/Thr-binding proteins dynamically regulates the functions of various client proteins involved in diverse biological processes (1). Whereas vertebrates express seven distinct 14-3-3 proteins ($\beta$, $\gamma$, $\varepsilon$, $\zeta$, $\eta$, $\sigma$, and $\tau$), only two isoforms exist in *Drosophila melanogaster* ($\varepsilon$ and $\zeta$), belonging to the two main 14-3-3 conservation groups (2). Structurally, 14-3-3 orthologues are very similar, as they adopt a dimeric U-shaped configuration with amphipathic grooves capable of accommodating two phosphorylated peptides (3). This feature allows 14-3-3 proteins to simultaneously bind two phosphorylated residues on one or two target proteins, thereby acting as scaffolding molecules. 14-3-3 proteins recognize the consensus sequence motifs RXX(pS/T)XP and RXXX(pS/T)XP (where X is any amino acid) in client proteins (4). However, phosphorylation-dependent sites that diverge significantly from these motifs have been described, with some 14-3-3 interaction being independent of phosphorylation (5). Molecularly, 14-3-3 binding may allosterically stabilize conformational changes, leading to activation or deactivation of the target or to interaction between two proteins (6). Furthermore, 14-3-3 binding may mask or expose interaction sites, often leading to changes in the subcellular localization of client proteins (7). While there are bound to be kingdom-specific 14-3-3 functions, the high level of structural conservation between 14-3-3 orthologues suggests that they regulate core cellular processes through evolutionarily conserved protein-protein interactions.

**Received** 11 May 2016 **Returned for modification** 18 June 2016 **Accepted** 11 November 2016

**Accepted manuscript posted online** 21 November 2016

**Citation** Laflamme C, Galan JA, Ben El Kadhi K, Méant A, Zeledon C, Carréno S, Roux PP, Emery G. 2017. Proteomics screen identifies class I Rab11 family interacting proteins as key regulators of cytokinesis. Mol Cell Biol 37:e00278-16. https://doi.org/10.1128/MCB.00278-16.



Address correspondence to Philippe P. Roux, philippe.roux@umontreal.ca, or Gregory Emery, gregory.emery@umontreal.ca.

* Present address: Carl Laflamme, Department of Neurology and Neurosurgery, Montreal Neurological Institute, McGill University, Montreal, Quebec, Canada; Jacob A. Galan, Department of Molecular Biology, Massachusetts General Hospital, Boston, Massachusetts, USA.

C.L., J.A.G., and K.B.E.K. contributed equally to this article.

Rab GTPases constitute a large family of proteins that regulate all stages of intracellular membrane trafficking (8). When they are active, Rab proteins interact with downstream effectors, which then perform diverse cellular functions necessary for vesicle formation, motility, docking, and fusion. Members of the Rab11 subfamily (Rab11a, Rab11b, and Rab25) localize to the endosomal recycling compartment and have been implicated in a variety of biological process, including cell division (9). Rab11 function is mediated by several effector proteins, including the Rab11 family interacting proteins (Rab11-FIPs; also known as FIPs). The FIPs constitute an evolutionarily conserved family of Rab11 effectors known to bridge from Rab GTPases to different molecular motors, ensuring vesicle motility (10). The FIPs are divided into two different classes, based on whether they possess phospholipid-binding C2 domains (class I) or EF-hand domains (class II) (10). Mammalian class I FIPs (FIP1, FIP2, and FIP5) are involved in polarized transport of cargos during epithelial cell polarity and are known to be regulated through phosphorylation (11–14). Rip11 is the only class I FIP in *Drosophila* and was shown to be involved in rhodopsin transport to the apical surface of photoreceptor cells (15) and in E-cadherin trafficking during trachea formation (16). Mammalian class II FIPs (FIP3 and FIP4) and their *Drosophila* orthologue Nuf are well-established regulators of cytokinesis (17–20). While the repertoire of FIP functions is expanding, much work is still required to understand the mechanisms regulating their activity.

Cytokinesis is the final step of cell division and leads to the physical separation of the daughter cells. After ingression of the cleavage furrow, future daughter cells remain connected by an intercellular bridge that is cleaved by a process called abscission. This process was shown to involve membrane trafficking, membrane fission (21), and lipid and cytoskeleton remodeling (22, 23).

Here we present the results of a proteomics screen aimed at characterizing the interactomes of 14-3-3 orthologues in multiple species. In total, we identified 141 proteins that interact with 14-3-3 in both human and *Drosophila* cells, suggesting that they regulate core and evolutionarily conserved biological processes. Among these, we identified all human class I FIPs (FIP1, -2, and 5) and their *Drosophila* orthologue Rip11 and found that 14-3-3 directly binds phosphorylated T391 and S405 in Rip11. We show that this interaction is required for successful cytokinesis in *Drosophila* cells, while binding to Rab11 is dispensable. 14-3-3 was previously shown to be involved in the regulation of protein synthesis during mitosis (24) and in preventing the centralspindlin complex, an essential protein complex involved in central spindle assembly (25–27), from oligomerizing *in vitro* (28). Our results describe a new 14-3-3 function during cytokinesis and suggest that it is part of an evolutionarily conserved pathway that controls important vesicular trafficking events during late cytokinesis.

## RESULTS

**Proteomics-based strategy to identify evolutionarily conserved 14-3-3 client proteins.** To characterize the 14-3-3 interactome in cells from different organisms, we devised an affinity-based approach using the $\varepsilon$ and $\zeta$ isoforms of 14-3-3, which are the only two isoforms present in both humans and *Drosophila*. To specifically identify phosphorylation-dependent binders, we mutated a conserved residue (Lys49 in human 14-3-3$\varepsilon$) present in all 14-3-3 orthologues which is involved in creating a salt bridge with the phosphorylated residue of client proteins (29). These 14-3-3 mutants (K49E) were used in subtractive fractionation steps in which nonspecific (glutathione *S*-transferase [GST] alone) and non-phospho-dependent (GST–14-3-3$^{K49E}$) interactions were removed (Fig. 1A). As a source of client proteins, we used lysates of *Drosophila* S2 and HEK293 cells growing in serum, which were subjected to 14-3-3 affinity purification with both wild-type (wt) and K49E mutant 14-3-3 proteins. Following stringent washes in high-salt buffers, associated proteins were eluted, precipitated, and resolved by SDS-PAGE (Fig. 1A and B). To determine whether our method could specifically enrich 14-3-3 client proteins, we used a phospho-motif antibody that detects the phosphorylated 14-3-3 binding sequence RXX(pS/T)XP. As expected, we found that proteins

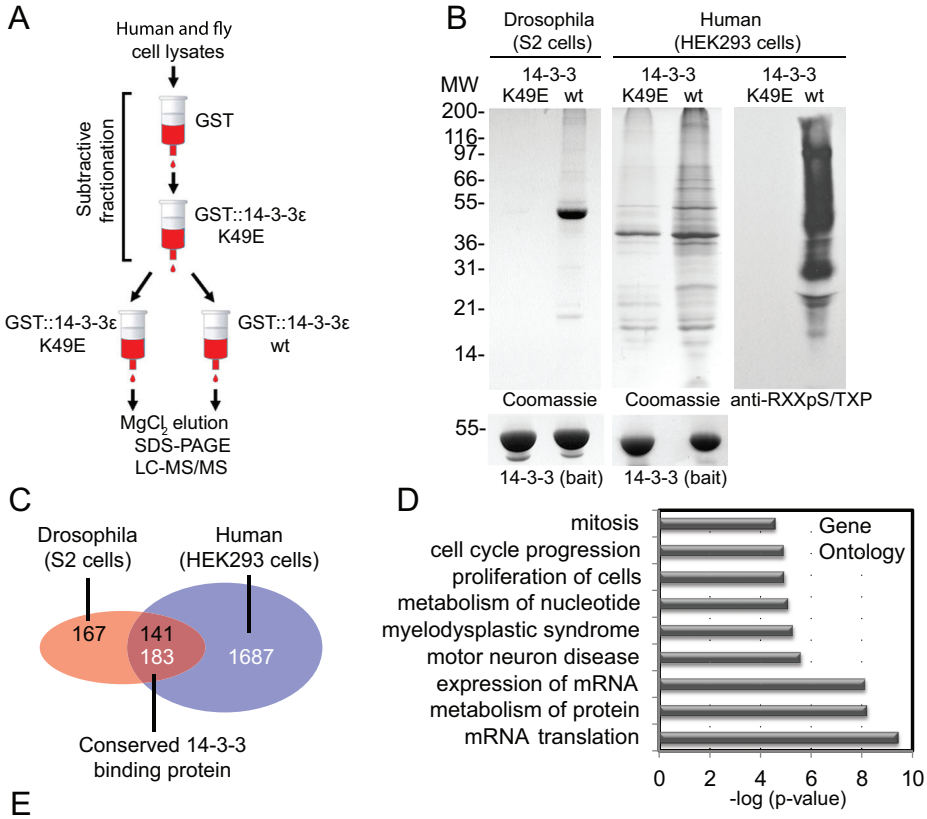


E

| No. | Accession | Fly name | Drosophila Function | Peptides | Accession | Human name | Peptides |
|---|---|---|---|---|---|---|---|
| 1 | Q9VWS3 | Rip11 | rhabdomere development | 19 | Q9BXF6 | RAB11FIP5 | 9 |
| 2 | Q9VEN1 | cheerio | mitosis, protein localization | 16 | P21333 | FLNA | 22 |
| 3 | Q8SYE5 | eIF3-S10 | mitotic spindle elongation | 11 | Q14152 | EIF3A | 9 |
| 4 | Q6NR71 | Hsp60 | mitochondrion organization | 10 | P10809 | HSPD1 | 27 |
| 5 | Q7KQ11 | eIF4G | G1/S transition of mitotic cell cycle | 10 | O43432 | EIF4G3 | 2 |
| 6 | O77285 | alphaCop | male meiosis cytokinesis | 9 | P53621 | COPA | 7 |
| 7 | Q9VPX6 | capt | actin polymerization, cell shape | 8 | Q01518 | CAP1 | 2 |
| 8 | P19109 | Rm62 | Alternative mRNA splicing | 8 | Q92841 | DDX17 | 1 |
| 9 | A4V2B8 | CkIIalpha | unknown | 8 | P68400 | CSNK2A1 | 2 |
| 10 | Q540W2 | Chc | regulation of growth | 7 | Q00610 | CLTC | 6 |
| 11 | P32234 | 128up/DRG1 | unknown | 7 | Q9Y295 | DRG1 (NEDD3) | 5 |
| 12 | Q95U75 | par-1 | border follicle cell migration | 7 | P27448 | MARK3 | 10 |
| 13 | P37276 | Dhc64C | axon cargo transport | 7 | Q14204 | DYNC1H1 | 2 |
| 14 | Q9V397 | Mtpalpha | determination of adult lifespan | 6 | P40939 | HADHA | 4 |
| 15 | A4V1C0 | RpL8 | translation elongation | 5 | P62917 | RPL8 | 4 |

**FIG 1** Proteomics-based strategy to characterize the 14-3-3 phosphorylation-dependent interactome. (A) Scheme depicting the subtractive fractionation strategy used to enrich phosphorylation-dependent 14-3-3 binding proteins. (B) Following the protocol shown in panel A, eluates were resolved by SDS-PAGE and gels were stained with Coomassie blue or subjected to immunoblotting using a 14-3-3 binding motif antibody (RXXpS/TXP). MW, molecular weight. (C) Venn diagram for comparison of proteomic identifications between fly (black numbers) and mammalian (white numbers) data sets. (D) Gene Ontology (GO) term enrichment of orthologous 14-3-3 interactors. (E) Partial list of known (green arrows) and unknown conserved 14-3-3 client proteins identified in this study. The red arrow indicates Rip11 and its orthologues.

eluted from wt 14-3-3 were highly immunoreactive to the phospho-motif antibody, whereas no signal could be detected in proteins eluted from the K49E mutant (Fig. 1B).

Having validated our approach, we performed large-scale experiments using both human and *Drosophila* 14-3-3$\varepsilon$ and -$\zeta$. Eluates for both wt and mutant 14-3-3 proteins were resolved by SDS-PAGE, proteins were in-gel digested with trypsin, and peptides were analyzed by liquid chromatography-mass spectrometry (LC-MS). Although some of the proteins found to interact with the 14-3-3 K49E mutant may be phospho-independent binders, they were removed from our analyses to focus on phosphorylation-dependent interactions. While we initially intended to identify isoform-specific binders of 14-3-3, we found that both the $\zeta$ and $\varepsilon$ isoforms were

capable of forming homo- and heterodimers with endogenous 14-3-3 isoforms, which prevented us from determining isoform-specific interactions. Nevertheless, our approach led to the identification of 1,842 and 308 proteins that bound to human and *Drosophila* 14-3-3 proteins, respectively (Fig. 1C; see Tables S1 and S2 in the supplemental material). Notably, we found that nearly 50% of identified *Drosophila* proteins were also identified in the human counterparts as one or multiple orthologues, corresponding to 141 orthologous 14-3-3 binding partners (Table S3). To characterize the global signature of the evolutionarily conserved 14-3-3 interactome, we used the Ingenuity Pathway Analysis (IPA) platform. We found enrichments of several cellular and molecular functions, including mRNA translation ($P < 3.8E-10$), nucleotide metabolism ($P < 8.4E-06$), and mitosis ($P < 2.8E-05$) (Fig. 1D). Taken together, these data revealed many conserved 14-3-3 interactions and shed new light on unexplored 14-3-3 functions related to fundamental biological processes.

**Class I FIPs are conserved 14-3-3 binding proteins.** The most abundant 14-3-3 binding protein identified for *Drosophila* cells was Rip11, a member of the class I Rab11-FIPs (Fig. 1E). All three human orthologues of Rip11 (FIP1, FIP2, and FIP5) were also identified in our proteomics screen (Fig. 2A), suggesting that class I FIPs are important 14-3-3 binding proteins. Notably, none of the orthologous members of the class II FIPs were identified in our study (Fig. 2A). Accordingly, only class I FIPs were confirmed to be 14-3-3 binding proteins in human cells (Fig. 2B). To ascertain that this interaction was indeed phosphorylation dependent, we tested the association of human FIP5 (Fig. 2C), the class I FIP with the highest sequence coverage in the proteomics screen, and *Drosophila* Rip11 (Fig. 2D) with wt and K49E mutant 14-3-3$\varepsilon$ proteins. We found that the binding of these two orthologous class I FIPs was almost completely abrogated by the K49E mutation, suggesting that the interaction requires prior phosphorylation (Fig. 2C and D). These results were extended by showing that recombinant 14-3-3$\varepsilon$ interacts directly with human FIP5 or *Drosophila* Rip11 by far-Western analysis (Fig. 2E and F). Notably, we found that $\lambda$-phosphatase treatment of human FIP5 and *Drosophila* Rip11 abrogated 14-3-3$\varepsilon$ binding, confirming the need for class I FIP phosphorylation (Fig. 2E and F). We then assessed if the interaction between FIP5 and 14-3-3 could be detected in cells by performing immunoprecipitation of myc-tagged FIP5 and hemagglutinin (HA)-tagged 14-3-3 isoforms (Fig. 2G). We found that FIP5 was able to bind to 14-3-3$\beta$ and 14-3-3$\sigma$, but we could not detect an interaction with either 14-3-3$\gamma$ or 14-3-3$\zeta$. Finally, we determined whether 14-3-3$\varepsilon$ binding to class I FIPs could be outcompeted by the R18 peptide (PHCVPRDLSWLDLE ANMCLP), which binds to the same amphipathic groove on the surface of 14-3-3 as that for phosphorylated peptides (30, 31). Consistent with our previous observations, we found that increasing concentrations of the R18 peptide inhibited human FIP5 and *Drosophila* Rip11 binding to 14-3-3$\varepsilon$ (Fig. 2H and I). Together, these data demonstrate that class I FIPs are specific binding partners of 14-3-3 and that these interactions require their phosphorylation in cells.

**14-3-3 interacts with the RBD of Rip11 via Thr391 and Ser405.** To determine the region within Rip11 involved in 14-3-3 binding, we generated various N-terminal and C-terminal deletion mutants of Rip11 fused to green fluorescent protein (GFP) (Fig. 3A). These mutants were expressed in *Drosophila* S2 cells to evaluate their interaction with 14-3-3$\varepsilon$ in pulldown assays. Notably, we found that only Rip11 fragments containing the Rab11 binding domain (RBD; amino acids [aa] 352 to 409) associated with 14-3-3$\varepsilon$ (Fig. 3B), indicating that this domain contains phosphorylated residues involved in 14-3-3 binding. Sequence analysis of the RBD by use of the prediction software 14-3-3-Pred (32) revealed two potential 14-3-3 binding sites, containing Thr391 [RVME(pT)HP] and Ser405 [RTT(pS)] (Fig. 3A). These residues were mutated to unphosphorylatable residues (T391A, S405A, and T391A/S405A [TS/AA] mutations), and the resulting mutants were tested for the ability to interact with 14-3-3 in a pulldown assay. While both single point mutants (T391A and S405A) retained the ability to interact with 14-3-3$\varepsilon$, we found that mutation of both sites strongly reduced 14-3-3$\varepsilon$ binding

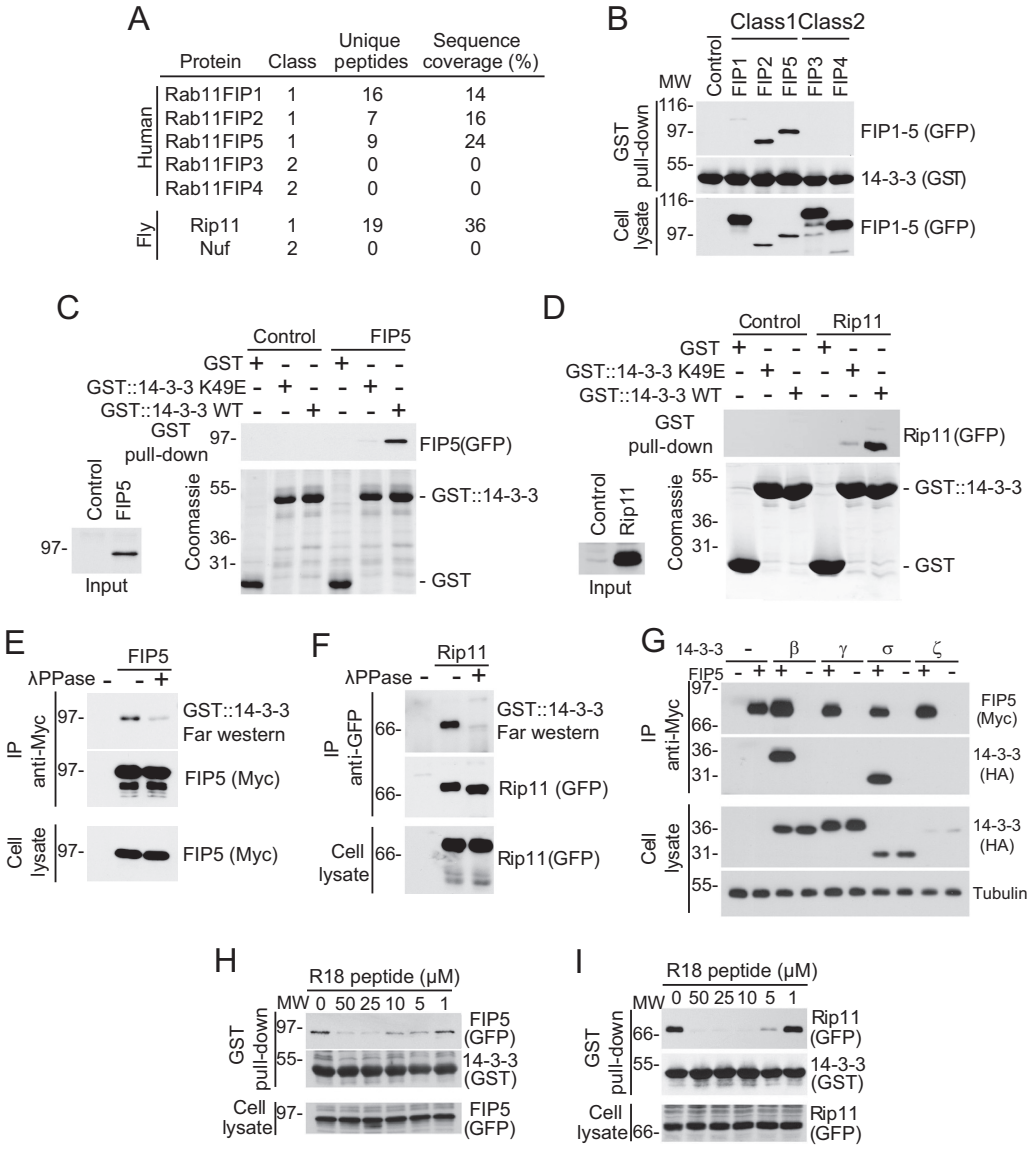


**FIG 2** Class I FIPs are conserved 14-3-3 binding proteins. (A) Numbers of unique peptides and sequence coverage for class I and class II FIPs in the proteomic analysis of 14-3-3 interactors. (B) Lysates of HEK293 cells expressing GFP-tagged forms of mammalian class I and class II FIPs were incubated with GST::14-3-3ε. After GST pulldown, 14-3-3 binding was analyzed by immunoblotting. (C) Lysates of HEK293 cells expressing GFP::FIP5 were incubated with GST::14-3-3ε and GST::14-3-3$\varepsilon^{K19E}$. Binding to both forms of 14-3-3 was analyzed by immunoblotting. Expression of FIP5 was assessed by immunoblotting of total cell lysate, whereas the amount of GST::14-3-3 was evaluated by Coomassie staining of SDS-PAGE gels. (D) Lysates of S2 cells expressing GFP::Rip11 were incubated with GST::14-3-3ε and GST::14-3-3$\varepsilon^{K49E}$, and binding was analyzed as described for panel C. (E) myc::FIP5 was immunoprecipitated (IP) from lysates of transfected HEK293 cells treated or not with λ-phosphatase (λPPase). Direct 14-3-3 binding was analyzed by far-Western blotting with purified GST::14-3-3ε. (F) GFP::Rip11 was immunoprecipitated from lysates of transfected S2 cells treated or not with λ-phosphatase (λPPase). Direct 14-3-3ε binding was analyzed as described for panel E. (G) myc::FIP5 was immunoprecipitated from lysates of HEK293 cells transfected with the indicated constructs. 14-3-3 binding was analyzed by immunoblotting. (H) Lysates of HEK293 cells expressing GFP::FIP5 were incubated with increasing concentrations of the R18 peptide, and FIP5 binding to 14-3-3ε was analyzed as described for panel B. (I) Lysates of S2 cells expressing GFP::Rip11 were incubated with increasing concentrations of the R18 peptide, and Rip11 binding to 14-3-3ε was analyzed as described for panel B.

(Fig. 3C), indicating that both T391 and S405 are required for this phospho-dependent interaction.

To address if T391 and S405 are involved in 14-3-3 binding in cells, we expressed myc-tagged 14-3-3ε together with GFP-tagged Rip11 constructs in S2 cells and proceeded to perform coimmunoprecipitation assays. While Rip11$^{WT}$ was efficiently coimmunoprecipitated with 14-3-3ε, we found that mutation of both T391 and S405 (TS/AA)

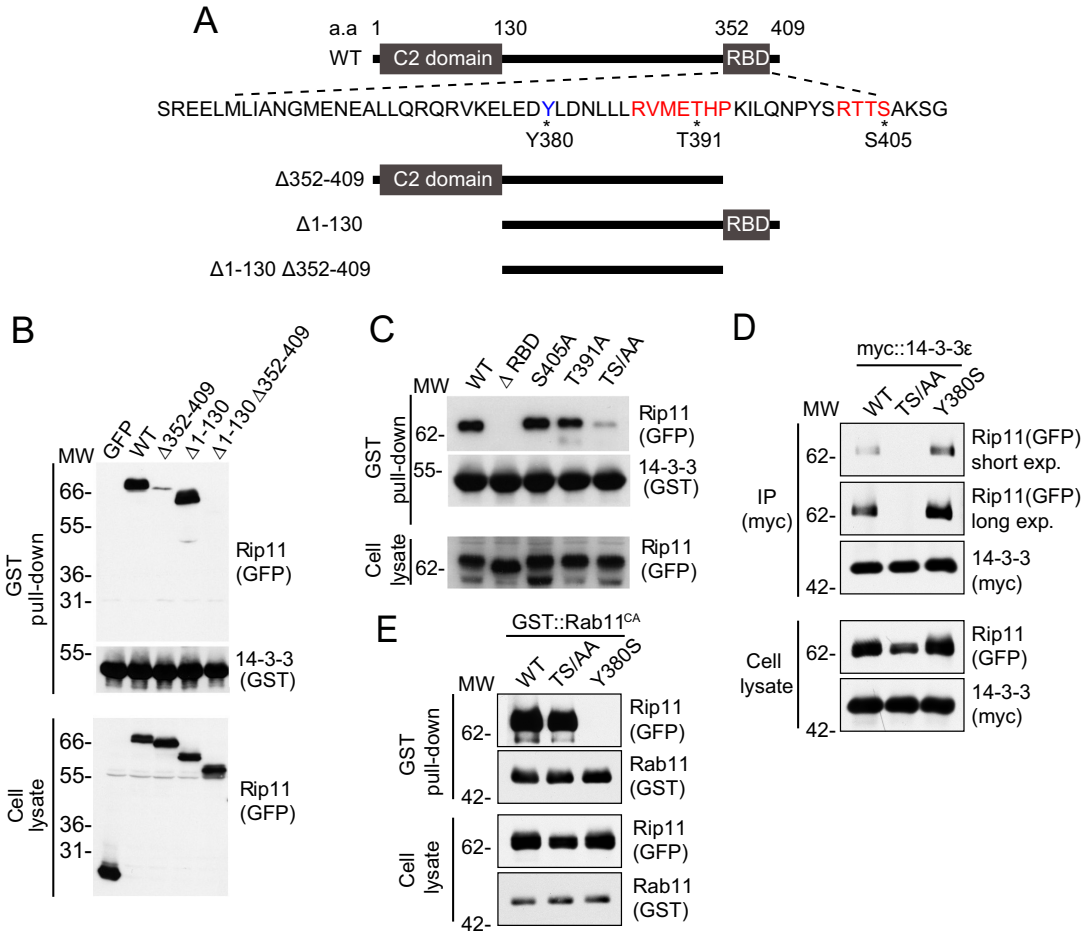


**FIG 3** 14-3-3 binds to T391 and S405 in the RBD of Rip11. (A) Schematic of the different GFP-tagged deletions and constructs of Rip11 that were generated for this study. Predicted 14-3-3 binding sites (in red) were determined by using the prediction software 14-3-3-Pred (32). The conserved Y380 residue involved in Rab11 binding is shown in blue. (B) Lysates of S2 cells expressing the indicated GFP-tagged Rip11 constructs were incubated with GST::14-3-3ε, and pulldown assays were performed and analyzed as described in the legend to Fig. 2B. (C) Lysates of S2 cells expressing the indicated GFP-tagged Rip11 constructs were incubated with GST::14-3-3ε, and pulldown assays were performed and analyzed as described for panel B. (D) myc::14-3-3ε was immunoprecipitated from lysates of S2 cells expressing the indicated GFP::Rip11 constructs and myc::14-3-3ε. Binding of the Rip11 variants was analyzed by immunoblotting. (E) Pulldown assays with lysates of S2 cells expressing the indicated GFP-tagged Rip11 constructs and GST::Rab11$^{CA}$ were analyzed by immunoblotting.

completely abolished this interaction (Fig. 3D). To verify if the loss of 14-3-3 binding was due to improper folding of the mutant Rip11 proteins, we tested their ability to interact with active Rab11 in a pulldown assay (33). As shown in Fig. 3E, we found that the TS/AA mutant of Rip11 retained the ability to interact with Rab11, indicating that mutation of T391 and S405 did not disrupt the overall structure of the RBD.

This observation prompted us to determine whether Rab11 binding to Rip11 is necessary for the Rip11–14-3-3 interaction. For this purpose, we mutated the conserved Y380 residue of Rip11 (Fig. 3A) to a serine residue (Y380S), which is predicted to disrupt Rip11 binding to Rab11 (34, 35). Accordingly, we found that this mutant lost the ability to interact with active Rab11 in pulldown assays (Fig. 3E). Next, we tested the ability of the Y380S mutant to interact with 14-3-3, and we found that Rab11 binding was not required for the interaction between Rip11 and 14-3-3 (Fig. 3D). Hence, these findings indicate that 14-3-3 interacts with Rip11 independently of Rab11.

**T391 and S405 are required for Rip11 distribution during cytokinesis.** To gain insights into the function of 14-3-3 binding to Rip11, we examined Rip11's endogenous localization in *Drosophila* S2 cells. While Rip11 appeared to be recruited to vesicles distributed throughout the cytoplasm of interphase cells, we found that its distribution

changed dramatically during mitosis. During metaphase, Rip11 vesicles were located in the vicinity of the plasma membrane and were redistributed close to the site of furrow ingression and on the central spindle during early telophase (Fig. 4A). In mid- to late telophase, Rip11 vesicles were enriched on the central spindle, near the cleavage furrow and at the intercellular bridge (Fig. 4A), and appeared to be mostly Rab11 positive (Fig. 4B).

We next investigated whether 14-3-3 binding is involved in the localization of Rip11 during mitosis. For this purpose, we performed time-lapse microscopy using S2 cells stably expressing GFP-tagged Rip11 constructs. This system appeared to be suitable for localization studies, as the distribution of GFP::Rip11$^{WT}$ was found to be similar to that of endogenous Rip11 (Fig. 4A and C). Interestingly, we found that GFP::Rip11$^{TS/AA}$ was also recruited to vesicles enriched near the cleavage furrow during mid- and late telophase, but their distribution was more dispersed, with numerous GFP::Rip11$^{TS/AA}$ vesicles found close to the poles of dividing cells (Fig. 4C). To quantify the difference in localization at late telophase between the different Rip11 mutants, we determined the enrichment of the protein near the cleavage furrow by measuring the ratio of the mean GFP fluorescence of an area expanding 1 $\mu$m around the cleavage plane to the mean GFP fluorescence of the entire cell (Fig. 4D; Movie S1). We found a 2.7-fold enrichment of GFP::Rip11$^{WT}$, which dropped to 1.5-fold for GFP::Rip11$^{TS/AA}$ (Fig. 4D′; Movie S2). These results suggest that 14-3-3 binding promotes the accumulation of Rip11 at the cleavage furrow during late telophase.

**Rip11 is involved in late stages of cytokinesis.** The distribution of Rip11 during mitosis suggests a role during cytokinesis. To test this hypothesis, we depleted *Rip11* by use of RNA interference (RNAi) and quantified the percentage of multinucleated cells as a marker of cytokinesis failure. Depletion of *Rip11* by use of double-stranded RNA (dsRNA) sequences targeting either the coding sequence or the 5′ untranslated region (UTR) induced a rate of multinucleated cells of 24.4% or 18.8%, respectively (Fig. 5A and B). For succeeding experiments, we used the dsRNA targeting the 5′ UTR, as it allowed us to perform rescue experiments. Hence, we confirmed that this dsRNA efficiently depleted both Rip11 isoforms (Rip11-PA and Rip11-PB) by Western blotting of S2 cell protein lysates (Fig. 5C; Movies S3 and S4). Both isoforms comprise an N-terminal C2 domain and a C-terminal RBD, but Rip11-PA also contains a larger central region of unknown function.

To determine which cytokinesis step(s) is impaired by the depletion of *Rip11*, we performed time-lapse microscopy of S2 cells expressing both mCherry-tagged anillin and a GFP fusion to the regulatory light chain of myosin II (Sqh-GFP) as markers of the cytokinesis machinery (Fig. 5D) (36). We observed that cytokinesis failed in 20.4% of the cells depleted of *Rip11* ($n = 416$). In these cells, the cytokinesis furrow regressed 61 $\pm$ 23 min after formation of the midbody, indicating that Rip11 is involved in late stages of cytokinesis. Interestingly, we also observed that anillin and Sqh were aberrantly recruited to internal vesicles in 31.7% of the dividing cells depleted of *Rip11*. A majority (54.5%) of these cells failed to complete cytokinesis. This suggests that Rip11 is required for the progression of cytokinesis by regulating the localization of anillin and Sqh at the cleavage furrow.

**Rip11 function during cytokinesis depends on 14-3-3 binding.** To examine whether Rip11 function during cytokinesis requires 14-3-3 binding, we performed rescue experiments with *Drosophila* S2 cells subjected to *Rip11* RNAi. Cells were stably transfected with various dsRNA-insensitive GFP-tagged constructs of Rip11 (Fig. 6A), and the multinucleated phenotype was quantified. We found that expression of a GFP fusion to the shorter isoform of Rip11 (Rip11-PB; labeled GFP::Rip11$^{WT}$ here) rescued the phenotype, suggesting that it was fully functional during cytokinesis. Similarly, the single point mutant GFP::Rip11$^{S405A}$ efficiently rescued cytokinesis, while the single point mutant GFP::Rip11$^{T391A}$ only partially prevented this phenotype. Conversely, our results showed that expression of GFP::Rip11$^{TS/AA}$ completely failed to restore cytoki-

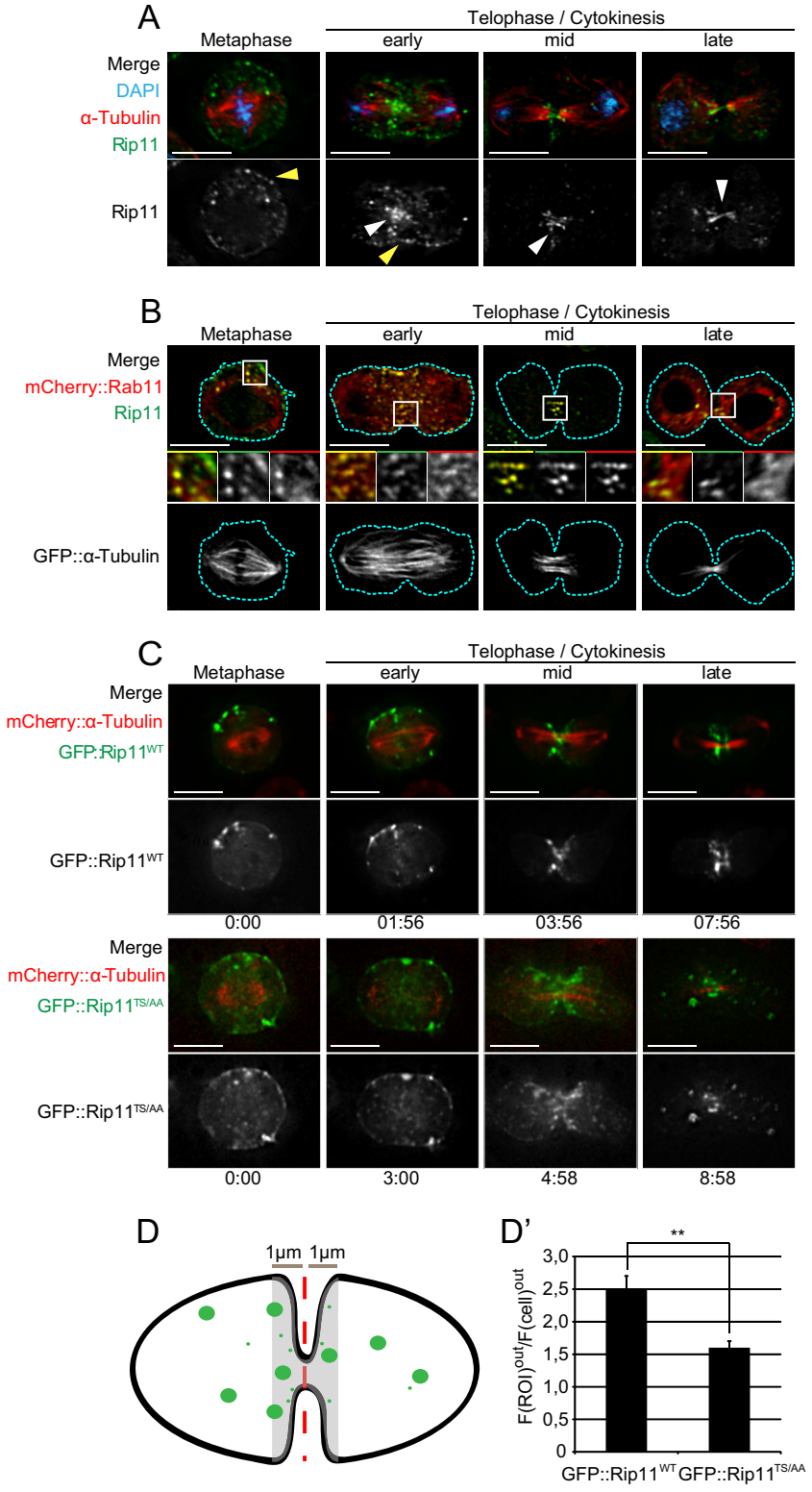


**FIG 4** T391 and S405 are required for Rip11 distribution at the cleavage furrow. (A) Representative images of endogenous Rip11 (green) at different stages of the cell cycle. Immunofluorescence assay of α-tubulin (red) and staining of the nucleus (DAPI; blue) were performed to identify the cell cycle stage. Grayscale images of the green channel are shown. White arrowheads point to Rip11 vesicles on the microtubule network, whereas yellow arrowheads point to vesicles close to the plasma membrane. Bars = 8 μm. (B) Representative examples of dividing S2 cells expressing mCherry::Rab11 (red) and GFP::tubulin (separated grayscale images) (lower panels) at the indicated cell cycle stages. Rip11 (green) was detected by immunofluorescence assay. High-magnification views of areas close to the plasma

(Continued on next page)

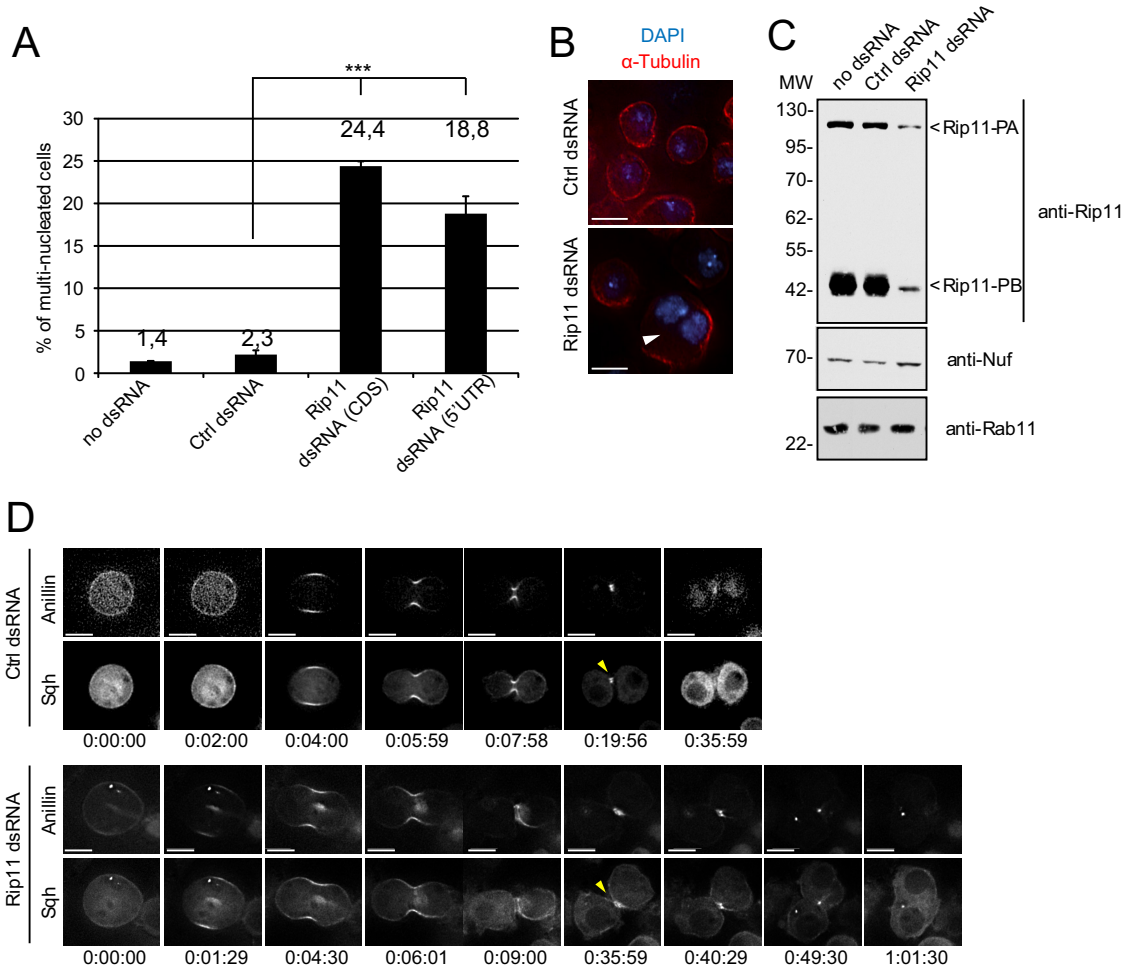


**FIG 5** Rip11 is required for late cytokinesis in S2 cells. (A) S2 cells were treated with the indicated dsRNA, and multinucleation was quantified. A minimum of 600 cells per condition were scored for 3 independent experiments (data are means and SD). Rip11 dsRNA (CDS), dsRNA targeting the coding sequence; Rip11 dsRNA (5′UTR), dsRNA targeting the 5′ untranslated region of *Rip11*. ***, $P < 0.001$. (B) Representative examples of control and *Rip11*-depleted S2 cells labeled with both F-actin (red) and DAPI (blue). The arrowhead indicates a binucleated cell. Bars = 8 $\mu$m. (C) The efficiency of the dsRNA targeting the 5′ UTR of *Rip11* was assessed by immunoblotting of lysates of S2 cells treated as indicated. (D) Selected frames showing representative dividing control or *Rip11*-depleted S2 cells expressing mCherry::anillin and Sqh::GFP. Arrowheads indicate the formation of the midbody. Bars = 8 $\mu$m.

nesis completion (Fig. 6A), suggesting that Rip11 function during cytokinesis requires its phosphorylation-dependent association with 14-3-3.

To determine whether constitutive 14-3-3 binding is sufficient to restore the function of Rip11 during cytokinesis, we fused GFP::Rip11$^{TS/AA}$ with the R18 sequence (GFP::Rip11$^{TS/AA}$::R18), which promotes 14-3-3$\varepsilon$ association independently of phosphorylation (Fig. 6B). Interestingly, although the R18 fusion abrogated Rab11 binding (Fig. 6C), it was able to significantly rescue cytokinesis upon Rip11 knockdown (Fig. 6A).

**FIG 4** Legend (Continued)
membrane or to the central spindle are shown with grayscale images of the red and green channels. Dashed lines delineate the cell perimeter. Bars = 8 $\mu$m. (C) Selected frames of dividing S2 cells expressing $\alpha$-tubulin::mCherry together with either GFP::Rip11$^{WT}$ (upper panels) or GFP::Rip11$^{TS/AA}$ (lower panels). Grayscale images of the green channel are shown. Bars = 8 $\mu$m. (D and D′) Enrichment of GFP::Rip11 at the cleavage furrow was calculated by dividing the background-corrected mean fluorescence intensity measured inside boundaries 1 $\mu$m from the plane of the cleavage furrow [F(ROI)$^{out}$] by the background-corrected mean fluorescence intensity measured in the whole dividing cell [F(cell)$^{out}$]. A total of 20 or 21 cells from 3 independent experiments were quantified for each condition (data show means and SEM). **, $P < 0.01$.

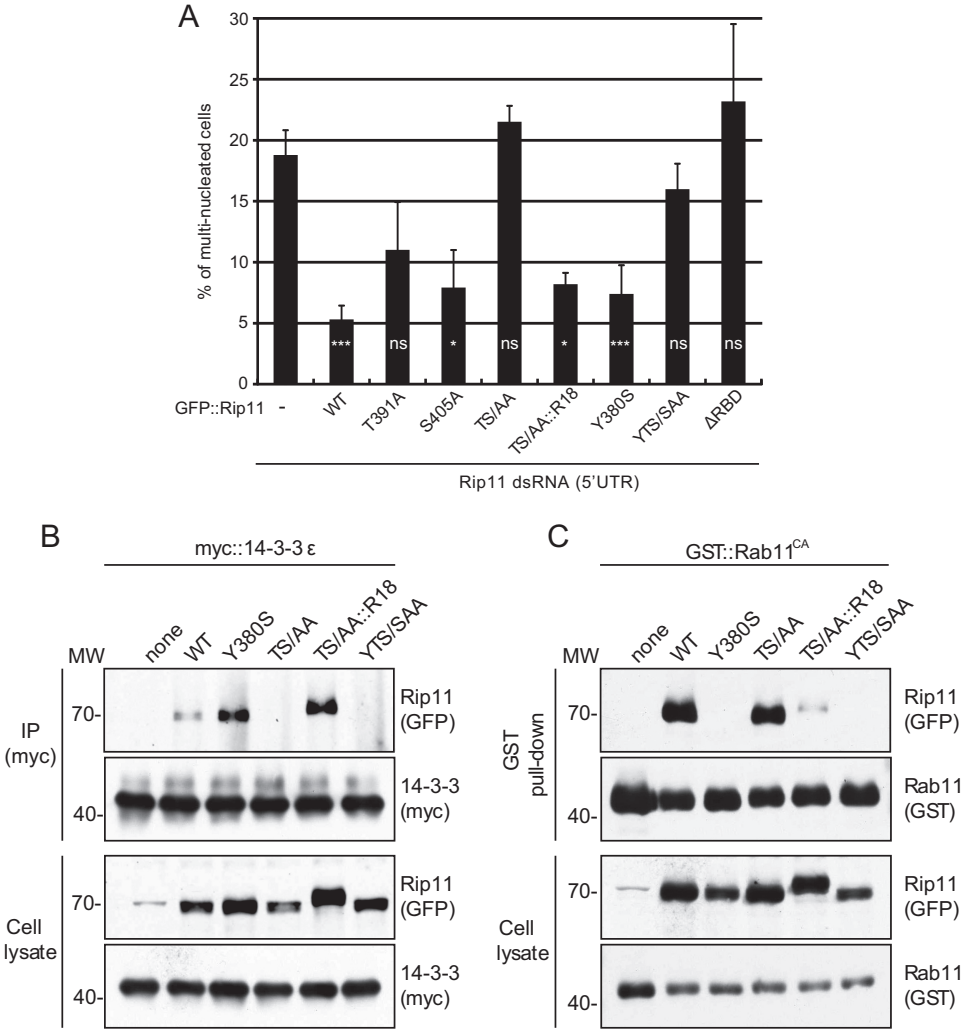


**FIG 6** Rip11 binding to 14-3-3 is required for completion of cytokinesis. (A) Control S2 cells (−) or cells stably expressing the indicated GFP-tagged Rip11 constructs were treated with dsRNA against *Rip11*, and multinucleation was quantified. A minimum of 500 cells per condition were scored for 2 or 3 independent experiments (data are means and SD). *, $P < 0.05$; ***, $P < 0.001$; ns, nonsignificant. (B) myc::14-3-3$\varepsilon$ was immunoprecipitated from lysates of S2 cells expressing the indicated GFP-tagged Rip11 constructs and myc::14-3-3$\varepsilon$. Binding of the Rip11 variants was analyzed as described in the legend to Fig. 3D. (C) GST pulldown assays were performed with lysates of S2 cells expressing the indicated GFP-tagged Rip11 variants and GST::Rab11$^{CA}$ and were analyzed as described in the legend to Fig. 3E.

These results support the notion that binding to 14-3-3 is necessary for Rip11 function during cytokinesis.

To confirm that the binding to Rab11 is dispensable for Rip11 function during cytokinesis, we expressed the Rab11 binding-deficient Rip11 mutant (Rip11$^{Y380S}$) and tested it for the ability to rescue cytokinesis in S2 cells depleted of *Rip11*. Importantly, we observed a complete cytokinesis rescue (Fig. 6A) with Rip11$^{Y380S}$, confirming that Rip11 acts independently of Rab11 binding for its function in cytokinesis.

To determine if the binding to 14-3-3 is required for Rip11 function in the absence of Rab11 binding, we expressed a Rip11 mutant deficient in both Rab11 and 14-3-3 binding through compounded point mutations (GFP::Rip11$^{YTS/SAA}$) (Fig. 6B and C). Similar to the results we obtained with GFP::Rip11$^{TS/AA}$ and GFP::Rip11$^{\Delta RBD}$, we found that these mutants failed to rescue cytokinesis in S2 cells depleted of *Rip11* (Fig. 6A). Hence, while all the previously described functions of Rip11 are dependent on Rab11 binding, its function during cytokinesis appears to be Rab11 independent and requires its interaction with 14-3-3.

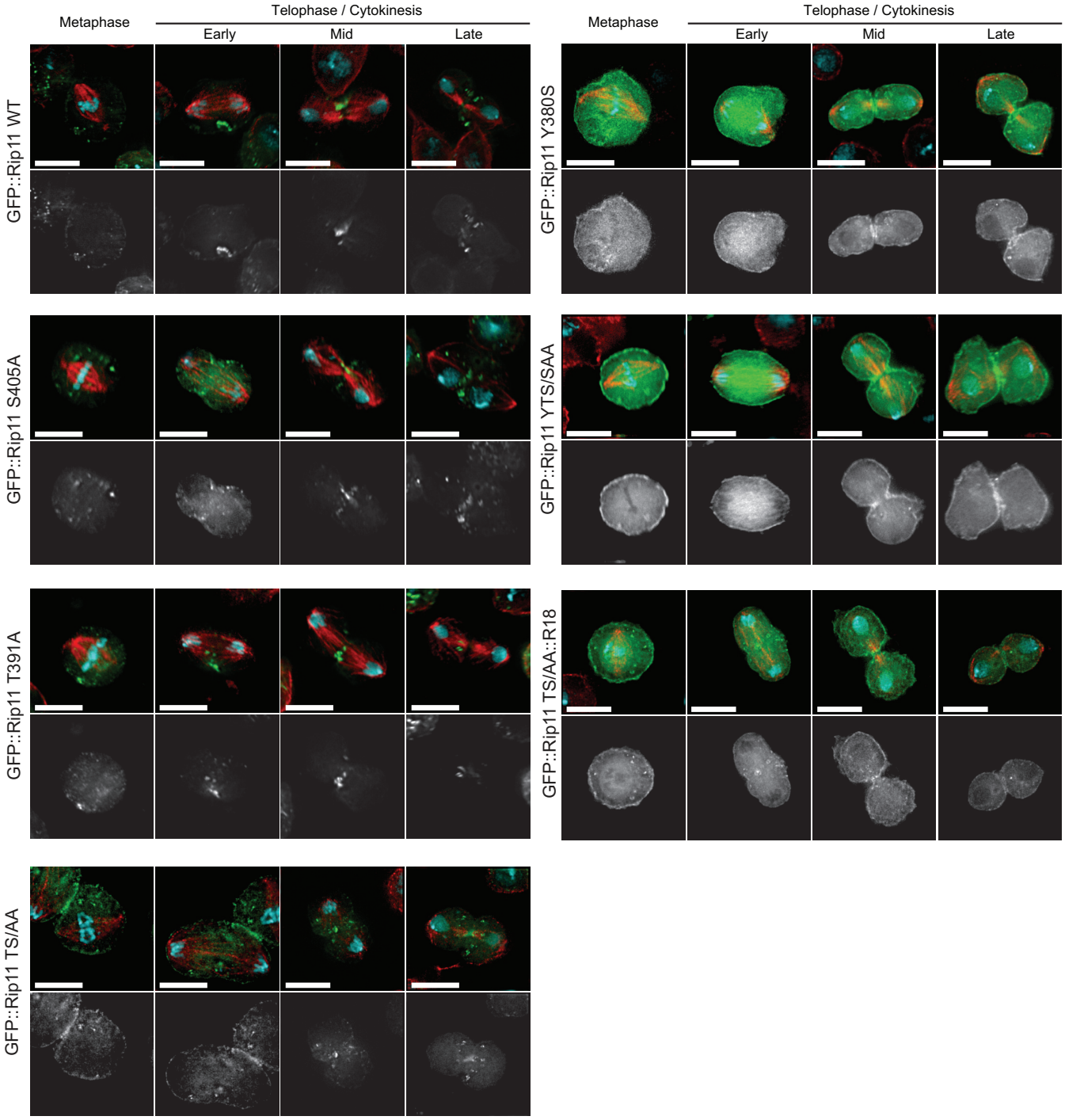


**FIG 7** Localization of Rip11 mutants during cytokinesis in rescue experiments. Representative images show S2 cells depleted of endogenous *Rip11* and expressing the indicated GFP-tagged Rip11 constructs (green) at the indicated stages of mitosis. Cells were labeled with $\alpha$-tubulin (red) and DAPI (blue). Bars = 10 $\mu$m.

Finally, as we previously found that the loss of binding to 14-3-3 changes the distribution of Rip11 vesicles (Fig. 4C and D), we imaged the different mutants of Rip11 in rescue experiments (Fig. 7). We found that GFP::Rip11$^{WT}$, GFP::Rip11$^{S405A}$, and GFP::Rip11$^{T391A}$ were present in vesicles close to the cytokinesis cleavage plane, while GFP::Rip11$^{TS/AA}$ vesicles were more dispersed. Both GFP::Rip11$^{Y380S}$ and GFP::Rip11$^{YTS/SAA}$ were found to be located mainly at the plasma membrane, including at the cleavage furrow, and occasionally on vesicles. Finally, GFP::Rip11$^{TS/AA}$::R18

was found both at the plasma membrane and on vesicles accumulating near the cleavage furrow.

## DISCUSSION

Several proteomics studies have characterized the 14-3-3 interactome in human cells, but at the moment, little is known about the identities of 14-3-3 client proteins in other organisms and their levels of conservation across species. Here we simultaneously characterized the 14-3-3 interactomes in human and fly cells, with the rationale that conserved 14-3-3 interactions will reveal regulatory mechanisms that control fundamental biological processes. Our screening strategy also enriched phosphorylation-dependent 14-3-3 client proteins, suggesting the involvement of a conserved set of kinases/phosphatases that regulates these interactions. Among identified proteins, we demonstrated that class I Rab11-FIPs are conserved 14-3-3 binding proteins and that this interaction is required for completion of cytokinesis. We found that 14-3-3 interacts with Rip11 via two phosphorylation sites located within its Rab11 binding domain but that Rab11 is dispensable for this newly characterized Rip11 function.

Rip11 was shown to interact with other Rab GTPases (37). Hence, it is possible that 14-3-3 regulates a function of Rip11 related to another Rab. A candidate screen performed in S2 cells revealed that Rab35 is an important regulator of cytokinesis (38), while in mammalian cells Rab35 was shown to ensure postfurrowing steps of cytokinesis by trafficking its effector OCRL to the intercellular bridge (38, 39). Previous work performed in HeLa cells linked 14-3-3 to the disassembly of the cytokinesis machinery (28, 40). In line with these findings, a role of Rip11/14-3-3 may be to regulate the trafficking of Rab35/Ocrl to allow the progression to abscission.

Some class I Rab11-FIPs were also shown to interact with myosin motors, such as kinesin-2 and myosin V, to promote protein trafficking (41, 42). Interestingly, kinesin-2 was shown to be involved in the delivery of Rab11-FIP5 to the cleavage furrow of epithelial cells (43), but whether Rip11 associates with kinesin-2 or another motor protein is currently unknown. Alternatively, 14-3-3 might regulate the C2 domain of Rip11 and its capacity to bind phospholipids, but more work will be required to assess these possibilities.

The function of 14-3-3 binding to Rip11 seems to be required at a precise time during cytokinesis, suggesting that its phosphorylation is tightly controlled. Identifying the kinase and/or phosphatase involved in Rip11 phosphorylation will be required to fully understand how its function is regulated. The basic residues located prior to T391 and S405 suggest the involvement of a basophilic kinase, such as protein kinase C (PKC). PKC was shown to have pleiotropic functions during mitosis (44), and although it is not impossible, determining its implication in the regulation of Rip11 function will likely be challenging.

In conclusion, our work led to the identification of a large number of 14-3-3 client proteins that are conserved across species. These results will be an important resource for future work on 14-3-3 proteins and the roles they play in fundamental processes, such as cell growth and division.

## MATERIALS AND METHODS

**Plasmid constructs.** Cloning of the different *Drosophila* constructs was done using Gateway technology (Invitrogen). We generated the different mutant forms of Rip11 by mutagenesis (QuikChange; Agilent) directly on Rip11$^{WT}$ (all the Rip11 constructs used in this study were generated from the Rip11$^{WT}$-PB isoform) in pDonor (33). We made the following Rip11 mutations: threonine 391 to alanine (T391A), serine 405 to alanine (S405A), and tyrosine 380 to serine (Y380S). The R18 peptide was fused directly after the last amino acid of Rip11$^{TS/AA}$. All Rip11 constructs were recombined in a copper-inducible pMET vector with a GFP tag at the N terminus to allow expression in *Drosophila* S2 cells (pMet-picoblast-GFP vector; a gift from V. Archambault [Université de Montréal, Montréal, Canada]). 14-3-3$\varepsilon$ was subcloned into pDonor and further recombined in the pAMW vector (actin promoter; myc tag at the N terminus). GST::Rab11$^{CA}$ and Rab11 were generated by use of the pDonor vector as previously described (33). Rab11 was recombined in pDest28 (UAS promoter; mCherry tag at the N terminus). GFP::tubulin was a gift from G. Hickson (Hôpital Sainte-Justine, Montréal, Canada).

Human FIP1, FIP2, FIP3, and FIP4 cloned into the p-EGFP-C1 plasmid for an N-terminal GFP tag were kind gifts from J. Goldenring (Vanderbilt University Medical Center, Nashville, TN), and human FIP5

cloned into the p-EGFP-C1 plasmid was a gift from M. W. McCaffrey (University College Cork, Cork, Ireland). FIP5 was cloned into pcDNA3 to introduce an N-terminal myc tag.

***Drosophila* S2 cell culture and dsRNA treatment.** *Drosophila* S2 cells were grown in Schneider's medium supplemented with 10% fetal bovine serum (FBS) supplemented with antibiotics. Stable cell lines were generated by transfecting the indicated constructs by use of Transit-LT1 transfection agent (Mirus). Blasticidin was used as a selection agent. mCherry::anillin- and Sqh::GFP-expressing S2 cells were obtained from the G. Hickson laboratory (45). For fixed samples, cells were cultured in a 96-well glass-bottomed plate (Greiner) for 6 days and treated with 3.5 $\mu$g of dsRNA at day 0 and day 3. For time-lapse microscopy, cells were cultured in a 96-well plate and treated with 3.5 $\mu$g of dsRNA at day 0 and 1 $\mu$g of dsRNA at day 3, and they were imaged at day 5.

dsRNAs were produced and used as previously described (46), using the following primers: for Gal4 control dsRNA, Gal4 forward (AGAAGTAAGGCGGTCGGGATAGT) and reverse (AGACACCAGCGAAATGGA TTTTT) primers; and for Rip11, CDS forward (CCGGCAAGGAGAAGAAGAAC) and reverse (GTTGCCGATGG ACAACAGAC) primers and 5′ UTR forward (CTACACTACGTTCTCCTGGCG) and reverse (CCTTTCGTTTCTT CTTCTTTGC) primers.

**Imaging of fixed samples, time-lapse recording, and quantifications.** For immunofluorescence assays and staining, we used mouse (1/200; Sigma) or rat (1/50; AbD Serotec) anti-$\alpha$-tubulin, rabbit anti-Rip11 (1/2,000; a gift from J. Casanova, Institut de Biologia Molecular de Barcelona-CSIC, Barcelona, Spain), and Alexa Fluor 488-phalloidin (1/100; Cell Signaling) for F-actin staining. DAPI (4′,6-diamidino-2-phenylindole; Sigma) was used to stain nuclei. Images were acquired using either a 63× (numerical aperture [NA] = 1.4) or 100× (NA = 1.42) planApo objective on a Deltavision microscope (Applied Precision) equipped with a CoolSnap HQ2 camera (Photometrics). Deconvolution was carried out using SoftWoRx software, version 5.5. Cells were fixed in 4% paraformaldehyde and then proceeded for immunostaining (46), while time-lapse imaging was performed in an environmental chamber at 25°C. All cell images represent a single focal plane. They were prepared for publication using Adobe Photoshop to adjust contrast, Gaussian blur, and levels and then assembled with Adobe Illustrator.

Quantifications of GFP::Rip11 were performed as follows. Using Adobe Photoshop, a rectangular selection box with a 2-$\mu$m width was created and aligned with the middle of the cleavage furrow of late-telophase cells. The extremities of the box were modified to overlap the boundaries of the cleavage furrow. The mean fluorescence of GFP::Rip11 was measured in this region of interest [F(ROI)] and in the whole dividing cells [F(cell)]. The fluorescence intensities of both F(ROI) and F(cell) were corrected by background subtraction [and then called $F(ROI)^{out}$ and $F(cell)^{out}$], and the ratio of $F(ROI)^{out}$ to $F(cell)^{out}$ was calculated to determine the enrichment of GFP::Rip11 at the cleavage furrow.

**Rescue experiments.** Stable S2 cell lines expressing the different GFP::Rip11 constructs under the control of the pMET promoter were treated with Rip11 5′ UTR dsRNA at day 0 and day 3 and incubated with 0.5 mM $CuSO_4$ at day 4 of treatment. At day 6, cells were fixed and $\alpha$-tubulin was stained. The number of normal bi- or multinucleated cells was quantified and represented in a histogram.

**Mammalian cell culture, treatments, and immunoprecipitation.** HEK293 cells were maintained at 37°C in Dulbecco's modified Eagle's medium (DMEM) with 4.5 g/liter glucose supplemented with 10% FBS and antibiotics. HEK293 cells were transfected using calcium phosphate precipitation as described previously (47). Cells were grown for 24 h after transfection and serum starved where indicated by using serum-free DMEM for an additional 16 to 18 h. Cell lysates were prepared as previously described (47). Briefly, cells were washed three times with ice-cold phosphate-buffered saline (PBS) and lysed in BLB (10 mM $K_3PO_4$, 1 mM EDTA, 5 mM EGTA, 10 mM $MgCl_2$, 50 nM $\beta$-glycerophosphate, 0.5% Nonidet P-40, 0.1% Brij 35, 0.1% deoxycholic acid, 1 mM sodium orthovanadate [$Na_3VO_4$], 1 mM phenylmethylsulfonyl fluoride [PMSF], and a Complete protease inhibitor cocktail tablet [Roche]). For immunoprecipitations, cell lysates were incubated with the indicated antibodies for 2 h, followed by a 1-h incubation with protein A–Sepharose CL-4B beads (GE Healthcare). Immunoprecipitates were washed three times in lysis buffer, and beads were eluted and boiled in 2× reducing sample buffer (5× reducing sample buffer contains 60 mM Tris-HCl, pH 6.8, 25% glycerol, 2% SDS, 14.4 mM 2-mercaptoethanol, and 0.1% bromophenol blue).

**14-3-3 immunoprecipitation and GST-Rab11 pulldown assays with S2 cells.** S2 cells were cotransfected by use of Transit-LT1 transfection agent (Mirus) with both GFP::Rip11 and myc::14-3-3$\varepsilon$ or GFP::Rip11 and GST::Rab11 constructs. GFP::Rip11 expression was induced by adding 0.5 mM $CuSO_4$ for 16 h, and cells were lysed in Nonidet P-40 lysis buffer (20 mM Tris, pH 8.0, 137 mM NaCl, 1% Nonidet P-40, 10% glycerol, and 1 mM EDTA) with protease and phosphatase inhibitors (48). For GST::$Rab11^{CA}$ pulldown assay, 50 $\mu$l of a 50% slurry of glutathione-Sepharose beads equilibrated in lysis buffer was added to protein lysates and rocked for 2 h at 4°C. For myc::14-3-3 immunoprecipitation, 1 $\mu$l of myc antibody (9E10) was added to the protein lysate and rocked for 2 h at 4°C. After incubation of cell lysates with antibodies, 50 $\mu$l of A/G beads (Santa Cruz Biotechnology) was added to the protein lysate for 1 h, and the mix was rocked at 4°C. Beads were washed four times with lysis buffer. Total protein lysates and eluted proteins were resolved by 10% SDS-PAGE and transferred to nitrocellulose membranes, and immunoblots were performed using the following antibodies: anti-GFP (1/1,000; Invitrogen), anti-GST (1/1,000; Cell Signaling), and anti-myc (9E10) (1/50,000). Stable S2 cell lines expressing different Rip11 variants were plated on day 1. GFP constructs were induced by adding 0.5 mM $CuSO_4$ for 8 h. Cells were lysed as described above and incubated with GST::14-3-3 beads. Beads were processed as described above.

**Purification of GST::14-3-3 fusion proteins, subtractive fractionation, and pulldown assays.** Fifty-milliliter overnight cultures of *Escherichia coli* BL21 transformed with pGEX-4T-14-3-3$\varepsilon$ wild type or K49E mutant (kindly provided by Bryan Ballif) (49) were diluted to 500 ml and induced with 1 mM IPTG

(isopropyl-β-D-thiogalactopyranoside) overnight at 25°C. Cells were pelleted and resuspended in 40 ml of bacterial lysis buffer (1× PBS, 10 mM EDTA, 0.1% Triton X, 1 mM PMSF, 1× protease inhibitor cocktail). Extracts were placed in 50-ml conical tubes on ice and sonicated using a probe sonicator six times for 30 s each, with 30-s delays between blasts. After sonication, the extracts were centrifuged at 13,000 × *g* for 30 min and aliquoted into 1-ml tubes to be stored at −80°C until further use. For subtractive fractionation, we used a previously described method (49). Briefly, serum-starved cells were lysed as described above. Cellular debris was removed by centrifugation for 10 min at 13,000 × *g*. The supernatant, corresponding to 20 mg of protein, was precleared by pouring it sequentially over glutathione-Sepharose (GE/Amersham/Pharmacia, Piscataway, NJ), glutathione-Sepharose bound to 500 μg of GST, and glutathione-Sepharose bound to 250 μg of GST::14-3-3ε K49E. The flowthrough was divided equally and poured over GST::14-3-3ε K49E (250 μg) or GST::14-3-3ε wild type (250 μg) (as shown in the schematic in Fig. 1A). The beads were then washed 2 times with 2 ml of lysis buffer, followed by a final wash of 2 ml of lysis buffer lacking Nonidet P-40 and Brij 35. Cellular proteins bound to each column were eluted stepwise with 400 μl of 400 mM $MgCl_2$ in 50 mM HEPES and 400 μl of 800 mM $MgCl_2$ in 50 mM HEPES and finally chased with 200 μl of 50 mM HEPES. Eluates were combined and precipitated with 15% trichloroacetic acid. Precipitated proteins were pelleted, washed with acetone, resuspended in reducing sample buffer, pH adjusted with a 1/6 volume of 1 M Tris base, boiled, and subjected to SDS-PAGE for Coomassie staining or immunoblotting. For smaller-scale GST pulldowns, cell lysates were incubated with 10 μg of GST::14-3-3ε wild type or K49E mutant for 2 h and washed four times with lysis buffer prior to elution with reducing sample buffer, SDS-PAGE, and immunoblotting.

**Sample preparation for mass spectrometry.** Coomassie-stained SDS-PAGE gels were cut at regions corresponding to specific molecular weights. Gel slices were treated with 10 mM dithiothreitol (DTT) and incubated for 1 h at 56°C, followed by alkylation with 15 mM iodoacetamide for 1 h at 25°C in the dark. Proteins were digested overnight with sequencing-grade modified trypsin (enzyme/protein ratio of 1:50) at 37°C. Digested peptides from gels were extracted, and the volume was reduced by use of a speed vacuum. All peptide samples were resuspended in 0.2% formic acid.

Fractionation was analyzed by online reverse-phase chromatography coupled with an electrospray ionization interface to acquire MS (measuring the intensity and *m/z* ratio for peptides) and MS/MS (giving fragmentation spectra of peptides) scans. A nanoflow high-pressure liquid chromatography (HPLC) system (Eksigent; Thermo Fisher Scientific) was used for online reverse-phase chromatographic separation; peptides were loaded into a 5-mm-long trap column (inner diameter, 300 μm) in buffer A (0.2% formic acid [FA]) and separated in an 18-cm-long fused silica capillary analytical column (inner diameter, 150 μm), both packed with 3 μm 200A Magic AQ $C_{18}$ reverse-phase material (Michrom). Peptides were eluted by increasing the concentration of buffer B (0.2% FA in acetonitrile [ACN]) from 5 to 40% in 100 min. Following the gradient elution, the column was washed with 80% buffer B and reequilibrated with 5% buffer B. Peptides were eluted into the mass spectrometer at a flow rate of 600 nl/min. The total run time was approximately 125 min, including sample loading and column conditioning. Peptides were analyzed using automated data-dependent acquisition on a LTQ-Orbitrap Elite mass spectrometer. Each MS scan was acquired at a resolution of 240,000 full width at half maximum (fwhm) (at 400 *m/z*) for the mass range of 300 to 2,000 Th, with the lock mass option enabled (*m/z* 445.120025), and was followed by up to 12 MS/MS data-dependent scans on the most intense ions by use of collision-induced activation (CID). AGC target values for MS and MS/MS scans were set to 1e6 (maximum fill time of 500 ms) and 1e5 (maximum fill time of 50 ms), respectively. The precursor isolation window was set to 2 Th, with a CID normalized collision energy of 35; the dynamic exclusion window was set to 60 s.

**Mass spectrometry data acquisition, quantitation analysis, and bioinformatics.** MS data were analyzed using MASCOT software and searched against the Uniprot/SwissProt subset for *Drosophila* (Drome) and human release 2014 (http://www.uniprot.org/). Search criteria included a static modification of cysteine residues of +57.0214 Da, with a variable modification of +15.9949 Da to include potential oxidation of methionines. Searches were performed with semitryptic digestion and allowed a maximum of two missed cleavages on the peptides analyzed from the sequence database. The false discovery rate (FDR) for peptide, protein, and site identification was set to 1%. Bioinformatics analysis was done with DAVID software.

**Statistical analysis.** Statistical significances were determined by two-tailed Student's *t* tests. Results are expressed as means ± standard errors of the means (SEM) or means ± standard deviations (SD), as indicated in the figure legends. Statistical significance was assumed for *P* values of $<0.05$.

## SUPPLEMENTAL MATERIAL

Supplemental material for this article may be found at https://doi.org/10.1128/MCB.00278-16.

**TEXT S1**, PDF file, 0.3 MB.
**VIDEO S1**, AVI file, 0.2 MB.
**VIDEO S2**, AVI file, 0.6 MB.
**VIDEO S3**, AVI file, 0.5 MB.
**VIDEO S4**, AVI file, 1.9 MB.

## ACKNOWLEDGMENTS

J.A.G. developed, performed, and analyzed the proteomics experiments related to the fly and human 14-3-3 interactomes, as well as all 14-3-3 pulldown assays and the

far-Western analysis. C.L. performed the molecular biology assays and *Drosophila* S2 cell culture, as well as the immunoprecipitation assays and Rab11 pulldown assays, together with C.Z. C.L. performed live-cell microscopy of Rip11 vesicles. K.B.E.K. performed live-cell imaging of Ani/Sqh cells, quantified multinucleated cells, and characterized the localization of the Rip11 mutants in rescue experiments. A.M. performed the FIP5 coimmunoprecipitations with HA-tagged 14-3-3. C.L., J.A.G., S.C., P.P.R., and G.E. wrote the manuscript.

We thank Jordi Casanova for the Rip11 antibody. We thank Gilles Hickson for helpful discussion and for reagents. We thank Vincent Archambault for Gateway plasmid reagents. We thank James Goldenring and Mary McCaffrey for providing mammalian FIP cDNAs.

This work was supported by Canadian Institutes of Health Research (CIHR) grants MOP133683 (to S.C.), MOP123408 (to P.P.R.), and MOP114899 (to G.E.), a grant from the Human Frontier Science Program (to P.P.R.), a Cancer Research Society grant (to G.E.), and an NSERC grant (to G.E.). S.C. holds a New Investigator Award from the CIHR. P.P.R. holds a Canada Research Chair in Cell Signaling and Proteomics and a Chercheur-Boursier award from the Fonds de la Recherche du Québec en Santé (FRQS). G.E. holds a Canada Research Chair in Vesicular Trafficking and Cell Signaling. C.L., K.B.E.K., and C.Z. held Ph.D. training awards from the FRQS. K.B.E.K. also held a Ph.D. fellowship from the Fondation Desjardins and a Ph.D. fellowship from the Fondation du Grand Défi Pierre Lavoie. J.A.G. held postdoctoral fellowships from the CIHR and FRQS.

## REFERENCES

1. Zhao J, Meyerkord CL, Du Y, Khuri FR, Fu H. 2011. 14-3-3 proteins as potential therapeutic targets. Semin Cell Dev Biol 22:705–712. https://doi.org/10.1016/j.semcdb.2011.09.012.
2. Wang W, Shakes DC. 1996. Molecular evolution of the 14-3-3 protein family. J Mol Evol 43:384–398. https://doi.org/10.1007/BF02339012.
3. Liu D, Bienkowska J, Petosa C, Collier RJ, Fu H, Liddington R. 1995. Crystal structure of the zeta isoform of the 14-3-3 protein. Nature 376:191–194. https://doi.org/10.1038/376191a0.
4. Gardino AK, Yaffe MB. 2011. 14-3-3 proteins as signaling integration points for cell cycle control and apoptosis. Semin Cell Dev Biol 22:688–695. https://doi.org/10.1016/j.semcdb.2011.09.008.
5. Obsil T, Obsilova V. 2011. Structural basis of 14-3-3 protein functions. Semin Cell Dev Biol 22:663–672. https://doi.org/10.1016/j.semcdb.2011.09.001.
6. Obsilova V, Kopecka M, Kosek D, Kacirova M, Kylarova S, Rezabkova L, Obsil T. 2014. Mechanisms of the 14-3-3 protein function: regulation of protein function through conformational modulation. Physiol Res 63(Suppl 1):S155–S164.
7. Reinhardt HC, Yaffe MB. 2013. Phospho-Ser/Thr-binding domains: navigating the cell cycle and DNA damage response. Nat Rev Mol Cell Biol 14:563–580. https://doi.org/10.1038/nrm3640.
8. Zerial M, McBride H. 2001. Rab proteins as membrane organizers. Nat Rev Mol Cell Biol 2:107–117. https://doi.org/10.1038/35052055.
9. Welz T, Wellbourne-Wood J, Kerkhoff E. 2014. Orchestration of cell surface proteins by Rab11. Trends Cell Biol 24:407–415. https://doi.org/10.1016/j.tcb.2014.02.004.
10. Horgan CP, McCaffrey MW. 2009. The dynamic Rab11-FIPs. Biochem Soc Trans 37:1032–1036. https://doi.org/10.1042/BST0371032.
11. Lapierre LA, Avant KM, Caldwell CM, Oztan A, Apodaca G, Knowles BC, Roland JT, Ducharme NA, Goldenring JR. 2012. Phosphorylation of Rab11-FIP2 regulates polarity in MDCK cells. Mol Biol Cell 23:2302–2318. https://doi.org/10.1091/mbc.E11-08-0681.
12. Ducharme NA, Hales CM, Lapierre LA, Ham AJ, Oztan A, Apodaca G, Goldenring JR. 2006. MARK2/EMK1/Par-1Balpha phosphorylation of Rab11-family interacting protein 2 is necessary for the timely establishment of polarity in Madin-Darby canine kidney cells. Mol Biol Cell 17:3625–3637. https://doi.org/10.1091/mbc.E05-08-0736.
13. Su T, Bryant DM, Luton F, Verges M, Ulrich SM, Hansen KC, Datta A, Eastburn DJ, Burlingame AL, Shokat KM, Mostov KE. 2010. A kinase cascade leading to Rab11-FIP5 controls transcytosis of the polymeric immunoglobulin receptor. Nat Cell Biol 12:1143–1153. https://doi.org/10.1038/ncb2118.
14. Li D, Mangan A, Cicchini L, Margolis B, Prekeris R. 2014. FIP5 phosphorylation during mitosis regulates apical trafficking and lumenogenesis. EMBO Rep 15:428–437. https://doi.org/10.1002/embr.201338128.
15. Li BX, Satoh AK, Ready DF. 2007. Myosin V, Rab11, and dRip11 direct apical secretion and cellular morphogenesis in developing Drosophila photoreceptors. J Cell Biol 177:659–669. https://doi.org/10.1083/jcb.200610157.
16. Shaye DD, Casanova J, Llimargas M. 2008. Modulation of intracellular trafficking regulates cell intercalation in the Drosophila trachea. Nat Cell Biol 10:964–970. https://doi.org/10.1038/ncb1756.
17. Schiel JA, Childs C, Prekeris R. 2013. Endocytic transport and cytokinesis: from regulation of the cytoskeleton to midbody inheritance. Trends Cell Biol 23:319–327. https://doi.org/10.1016/j.tcb.2013.02.003.
18. Wilson GM, Fielding AB, Simon GC, Yu X, Andrews PD, Hames RS, Frey AM, Peden AA, Gould GW, Prekeris R. 2005. The FIP3-Rab11 protein complex regulates recycling endosome targeting to the cleavage furrow during late cytokinesis. Mol Biol Cell 16:849–860.
19. Cao J, Albertson R, Riggs B, Field CM, Sullivan W. 2008. Nuf, a Rab11 effector, maintains cytokinetic furrow integrity by promoting local actin polymerization. J Cell Biol 182:301–313. https://doi.org/10.1083/jcb.200712036.
20. Riggs B, Rothwell W, Mische S, Hickson GR, Matheson J, Hays TS, Gould GW, Sullivan W. 2003. Actin cytoskeleton remodeling during early Drosophila furrow formation requires recycling endosomal components Nuclear-fallout and Rab11. J Cell Biol 163:143–154. https://doi.org/10.1083/jcb.200305115.
21. Mierzwa B, Gerlich DW. 2014. Cytokinetic abscission: molecular mechanisms and temporal control. Dev Cell 31:525–538. https://doi.org/10.1016/j.devcel.2014.11.006.
22. D'Avino PP, Giansanti MG, Petronczki M. 2015. Cytokinesis in animal cells. Cold Spring Harb Perspect Biol 7:a015834. https://doi.org/10.1101/cshperspect.a015834.
23. Green RA, Paluch E, Oegema K. 2012. Cytokinesis in animal cells. Annu Rev Cell Dev Biol 28:29–58. https://doi.org/10.1146/annurev-cellbio-101011-155718.
24. Wilker EW, van Vugt MA, Artim SA, Huang PH, Petersen CP, Reinhardt HC, Feng Y, Sharp PA, Sonenberg N, White FM, Yaffe MB. 2007. 14-3-3sigma controls mitotic translation to facilitate cytokinesis. Nature 446:329–332. https://doi.org/10.1038/nature05584.
25. Yuce O, Piekny A, Glotzer M. 2005. An ECT2-centralspindlin complex regulates the localization and function of RhoA. J Cell Biol 170:571–582. https://doi.org/10.1083/jcb.200501097.

26. Zhao WM, Fang G. 2005. MgcRacGAP controls the assembly of the contractile ring and the initiation of cytokinesis. Proc Natl Acad Sci U S A 102:13158–13163. https://doi.org/10.1073/pnas.0504145102.
27. Mishima M, Kaitna S, Glotzer M. 2002. Central spindle assembly and cytokinesis require a kinesin-like protein/RhoGAP complex with microtubule bundling activity. Dev Cell 2:41–54. https://doi.org/10.1016/S1534-5807(01)00110-1.
28. Douglas ME, Davies T, Joseph N, Mishima M. 2010. Aurora B and 14-3-3 coordinately regulate clustering of centralspindlin during cytokinesis. Curr Biol 20:927–933. https://doi.org/10.1016/j.cub.2010.03.055.
29. Zhang L, Wang H, Liu D, Liddington R, Fu H. 1997. Raf-1 kinase and exoenzyme S interact with 14-3-3zeta through a common site involving lysine 49. J Biol Chem 272:13717–13724. https://doi.org/10.1074/jbc.272.21.13717.
30. Wang B, Yang H, Liu YC, Jelinek T, Zhang L, Ruoslahti E, Fu H. 1999. Isolation of high-affinity peptide antagonists of 14-3-3 proteins by phage display. Biochemistry 38:12499–12504. https://doi.org/10.1021/bi991353h.
31. Petosa C, Masters SC, Bankston LA, Pohl J, Wang B, Fu H, Liddington RC. 1998. 14-3-3zeta binds a phosphorylated Raf peptide and an unphosphorylated peptide via its conserved amphipathic groove. J Biol Chem 273:16305–16310. https://doi.org/10.1074/jbc.273.26.16305.
32. Madeira F, Tinti M, Murugesan G, Berrett E, Stafford M, Toth R, Cole C, MacKintosh C, Barton GJ. 2015. 14-3-3-Pred: improved methods to predict 14-3-3-binding phosphopeptides. Bioinformatics 31:2276–2283. https://doi.org/10.1093/bioinformatics/btv133.
33. Laflamme C, Assaker G, Ramel D, Dorn JF, She D, Maddox PS, Emery G. 2012. Evi5 promotes collective cell migration through its Rab-GAP activity. J Cell Biol 198:57–67. https://doi.org/10.1083/jcb.201112114.
34. Jagoe WN, Lindsay AJ, Read RJ, McCoy AJ, McCaffrey MW, Khan AR. 2006. Crystal structure of rab11 in complex with rab11 family interacting protein 2. Structure 14:1273–1283. https://doi.org/10.1016/j.str.2006.06.010.
35. Shiba T, Koga H, Shin HW, Kawasaki M, Kato R, Nakayama K, Wakatsuki S. 2006. Structural basis for Rab11-dependent membrane recruitment of a family of Rab11-interacting protein 3 (FIP3)/Arfophilin-1. Proc Natl Acad Sci U S A 103:15416–15421. https://doi.org/10.1073/pnas.0605357103.
36. Kechad A, Jananji S, Ruella Y, Hickson GR. 2012. Anillin acts as a bifunctional linker coordinating midbody ring biogenesis during cytokinesis. Curr Biol 22:197–203. https://doi.org/10.1016/j.cub.2011.11.062.
37. Kelly EE, Horgan CP, Adams C, Patzer TM, Ni Shuilleabhain DM, Norman JC, McCaffrey MW. 2009. Class I Rab11-family interacting proteins are binding targets for the Rab14 GTPase. Biol Cell 102:51–62. https://doi.org/10.1042/BC20090068.
38. Kouranti I, Sachse M, Arouche N, Goud B, Echard A. 2006. Rab35 regulates an endocytic recycling pathway essential for the terminal steps of cytokinesis. Curr Biol 16:1719–1725. https://doi.org/10.1016/j.cub.2006.07.020.
39. Dambournet D, Machicoane M, Chesneau L, Sachse M, Rocancourt M, El Marjou A, Formstecher E, Salomon R, Goud B, Echard A. 2011. Rab35 GTPase and OCRL phosphatase remodel lipids and F-actin for successful cytokinesis. Nat Cell Biol 13:981–988. https://doi.org/10.1038/ncb2279.
40. Joseph N, Hutterer A, Poser I, Mishima M. 2012. ARF6 GTPase protects the post-mitotic midbody from 14-3-3-mediated disintegration. EMBO J 31:2604–2614. https://doi.org/10.1038/emboj.2012.139.
41. Schonteich E, Wilson GM, Burden J, Hopkins CR, Anderson K, Goldenring JR, Prekeris R. 2008. The Rip11/Rab11-FIP5 and kinesin II complex regulates endocytic protein recycling. J Cell Sci 121:3824–3833. https://doi.org/10.1242/jcs.032441.
42. Hales CM, Vaerman JP, Goldenring JR. 2002. Rab11 family interacting protein 2 associates with myosin Vb and regulates plasma membrane recycling. J Biol Chem 277:50415–50421. https://doi.org/10.1074/jbc.M209270200.
43. Li D, Kuehn EW, Prekeris R. 2014. Kinesin-2 mediates apical endosome transport during epithelial lumen formation. Cell Logist 4:e28928. https://doi.org/10.4161/cl.28928.
44. Brownlow N, Pike T, Crossland V, Claus J, Parker P. 2014. Regulation of the cytokinesis cleavage furrow by PKCepsilon. Biochem Soc Trans 42:1534–1537. https://doi.org/10.1042/BST20140240.
45. El Amine N, Kechad A, Jananji S, Hickson GR. 2013. Opposing actions of septins and Sticky on Anillin promote the transition from contractile to midbody ring. J Cell Biol 203:487–504. https://doi.org/10.1083/jcb.201305053.
46. Ben El Kadhi K, Roubinet C, Solinet S, Emery G, Carreno S. 2011. The inositol 5-phosphatase dOCRL controls PI(4,5)P2 homeostasis and is necessary for cytokinesis. Curr Biol 21:1074–1079. https://doi.org/10.1016/j.cub.2011.05.030.
47. Roux PP, Ballif BA, Anjum R, Gygi SP, Blenis J. 2004. Tumor-promoting phorbol esters and activated Ras inactivate the tuberous sclerosis tumor suppressor complex via p90 ribosomal S6 kinase. Proc Natl Acad Sci U S A 101:13489–13494. https://doi.org/10.1073/pnas.0405659101.
48. Laflamme C, Emery G. 2015. In vitro and in vivo characterization of the Rab11-GAP activity of Drosophila Evi5. Methods Mol Biol 1298:187–194. https://doi.org/10.1007/978-1-4939-2569-8_16.
49. Ballif BA, Cao Z, Schwartz D, Carraway KL, III, Gygi SP. 2006. Identification of 14-3-3epsilon substrates from embryonic murine brain. J Proteome Res 5:2372–2379. https://doi.org/10.1021/pr060206k.